Waves in stratified viscoelastic media with microstructure

Robert Burridge

Schlumberger-Doll Research, Old Quarry Road, Ridgefield, Connecticut 06877

Maarten V. de Hoopa)

Schlumberger Cambridge Research, High Cross, Madingley Road, Cambridge CB3 OEL, England

Kai Hsu

Schlumberger LWD Engineering, 225 Industrial Boulevard, Sugarland, Texas 77479

Lawrence Le

Department of Geology and Geophysics, The University of Calgary, 2500 University Drive, Calgary, Alberta T2N 1N4, Canada

Andrew Norris

Department of Mechanical and Aerospace Engineering, Rutgers University, Piscataway, New Jersey 08855-0909

(Received 5 May 1993; revised 25 July 1993; accepted 28 July 1993)

An extension of the O'Doherty and Anstey theory [R. F. O'Doherty and N. A. Anstey, Geophys. Prosp. 19, 430-458 (1971)] is derived for waves in finely layered, anisotropic, viscoelastic media. Multiple scattering effects cause the direct wave to be delayed and broadened, subject to a deterministic integrodifferential delay equation. The kernel depends upon time-domain autocorrelations of reflectivities and the relaxation functions defining the viscoelastic effects. The medium differs from a slowly varying medium by $O(\epsilon)$, and propagation over $O(1/\epsilon^2)$ distances is considered. Both smoothly varying media and interfaces are considered simultaneously. A regular perturbation technique is used to show how an approximation to the field may be rapidly calculated. The signal delay predicted by the theory is identified with the retardation (drift) in the equivalent effective medium for the same interval. Numerical examples using synthetic fractal media show the approximate solutions to be in very good agreement with exact computations but 30-30 000 times faster.

PACS numbers: 43.20.Bi, 43.20.Gp, 43.20.Jr, 43.35.Mr

INTRODUCTION

A pulse propagates obliquely through a perfectly stratified, isotropic, viscoelastic earth medium, over a vertical distance large compared with the length scale on which the medium varies. If the ratio of these lengths is e^{-2} , we shall assume the medium differs from a slowly varying medium by $O(\epsilon)$. We show by a perturbation technique how an approximation to the field may be rapidly calculated. The method is closely related to that of Burridge and Chang¹ and of De Hoop et al., but extends the region of validity further into the wave coda by using the sample autocorrelation instead of the theoretical, ensemble-averaged autocorrelation of reflectivity. In the numerical examples illustrating this naive theory we obtain very good agreement with exact computations using a layer-matrix code. The main error is a small but growing error of timing late in the coda. This may be corrected by using the travel times appropriate to the (local) effective medium throughout. A complete analysis of this correction has yet to be made. As the degree of variation in the medium ϵ increases, and as

The line of research followed in this paper was initiated by O'Doherty and Anstey³ and has been continued by various authors concerned with the time delay (drift) and the pulse broadening (stratigraphic filtering) caused by multiple scattering. Since similar effects are caused by anelasticity there is considerable interest in understanding and distinguishing the effects of multiple scattering from those of anelasticity. The present paper includes multiple scattering and anelasticity together so that their effects can be more easily compared.

For a fuller survey of earlier work with references, see Refs. 5 and 6. For a thorough discussion of the corresponding stochastic problem with emphasis on the reflected wave, see Ref. 7.

In Sec. I, the equations governing viscoelastic wave propagation in a stratified medium are set up. For sufficiently small fixed horizontal slowness p, the equations take the form of a one-dimensional, first-order, linear, hyperbolic system $\partial_z v + M(z)\partial_\sigma v = 0$, where $\sigma = t - px$, with t the (absolute) time. The matrix M, which is assumed to be piecewise differentiable with discrete jump discontinuities, is separated into two parts. One part represents the perfectly elastic, instantaneous response of the medium and

time into the coda increases, the accuracy decreases, but accuracy improves as the frequency of the input pulse is lowered.

a) Formerly at: Koninklijke/Shell Exploratie en Produktie Laboratorium Volmerlaan 6, 2288 GD Rijswijk ZH, The Netherlands.

contains the effects of scattering by inhomogeneity; the other involves the relaxation functions and represents an elasticity. The elastic part is diagonalized by means of an eigenvector decomposition. The resulting hyperbolic system must be supplemented by jump conditions at the interfaces, that is, at the points of discontinuity of M.

In Sec. II, the small parameter ϵ is introduced. After diagonalization the elastic scattering term is assumed to be $O(\epsilon)$ while the anelastic term is assumed to be $O(\epsilon)$. This ensures that the two effects will be comparable in the final analysis. The fastest downgoing mode, the P wave, is chosen for special attention and a comoving frame of reference is used that travels downward with the P wave speed. We postulate a solution in the form of a power series in ϵ and then obtain a closed integrodifferential equation with jump conditions for the amplitude of the mode of interest correct to $O(\epsilon^2)$. By introducing Dirac distributions with weights that may be interpreted as reflection and transmission coefficients, the jump conditions may be incorporated into the integrodifferential equation.

The connection with effective-medium theory is discussed in Sec. III. The signal delay, defined as the delay between the first arrival and the time of arrival of the centroid of the pulse, is identified with the characteristic arrival time of the effective medium.

In Sec. IV, some numerical examples are presented that show the accuracy of this approximate method. We calculate the impulse responses for several purely elastic synthetic Goupillaud media derived from fractals of the fractional Brownian motion type. The agreement with the exact solution is shown in several plots and is good, especially early in the signal, but deteriorates both with increasing time in the coda and as the magnitude of the reflection coefficients increases. The approximate computations were carried out by means of fast Fourier transforms, and were found to be 30-30 000 times faster than the finite-difference computations of the exact solution.⁵ Finally, we calculated the particle velocity corresponding to a smooth lowfrequency incident pulse in a different Goupillaud medium. We carry these computations farther into the coda than in the previous examples. Here there is very good agreement between the approximate and the exact solution even quite late in the coda, but there is a small progressive timing error at later times. However, this may be corrected by using effective medium travel times throughout instead of characteristic travel times.

I. THE BASIC EQUATIONS

Let x,y,z be spatial coordinates, with z vertically downward, perpendicular to the layering, and let t be the time. Assume that the properties of the medium are functions of z only, and that the particle velocities and stresses are functions of z and t-px only. Then it is known that the equations of elasticity in a continuously variable medium have the form

$$\partial_z v + M(z)\partial_\sigma v = 0, (1)$$

where v(z,t) is the vector of particle velocities and traction components across surfaces z= const, and M(z) is an $n\times n$ matrix of material parameters that are functions of the density, the elastic constants of the material, and the horizontal slowness p, and

$$\sigma = t - px. \tag{2}$$

When the material parameters have discrete jump discontinuities, Eq. (1) must be supplemented by the interface condition that v is continuous at the points of discontinuity of M. For isotropic elasticity the system splits into two decoupled systems, the 4×4 P-SV system for the in-plane components, and the 2×2 SH system for the out-of-plane components.

We now separate M into two parts, rewriting Eq. (1) as

$$\partial_z v + M_0 \, \partial_\sigma v + \partial_\sigma M_1 * v = 0. \tag{3}$$

Here, M_0 represents the instantaneous elastic response, M_1 involves the relaxation functions and accounts for the inelastic behavior, and * denotes convolution with respect to σ . The matrix M has the infinitesimal symplectic symmetries

$$M_0^T J = J M_0, (4a)$$

$$M_1^T J = J M_1, \tag{4b}$$

where

$$J = \begin{pmatrix} 0 & I_{n/2} \\ I_{n/2} & 0 \end{pmatrix}, \tag{5}$$

with $I_{n/2}$ the $(n/2) \times (n/2)$ identity matrix. Set

$$v(z,\sigma) = E(z)w(z,\sigma), \tag{6}$$

where E is the tensor of eigenvectors of M_0 defined by

$$M_0E=E\Lambda,$$
 (7)

with

$$\Lambda = \operatorname{diag}[\gamma_1, ..., \gamma_n]. \tag{8}$$

Thus

$$E=(e_1,...,e_n), (9)$$

where the vertical slownesses γ_k are the eigenvalues and the e_k are the eigenvectors of M_0 ; they are assumed to be real and nonzero. Let

$$s_k = \operatorname{sgn}(\gamma_k), \tag{10}$$

and

$$K = \operatorname{diag}[s_1, ..., s_n]. \tag{11}$$

We shall normalize the eigenvectors so that

$$E^T J E = K. (12)$$

Then mode k propagates in the direction of $s_k z$. Since $K^{-1} = K$, it follows that

$$E^{-1} = KE^T J. (13)$$

Using Eqs. (7), (8), and (13), we rewrite Eq. (3) in the form

$$K(\partial_z + \Lambda \partial_\alpha)w = -E^T J(\partial_z E)w - E^T J(\partial_\alpha M_1)E *w.$$
 (14)

From Eq. (12) and the fact that $\partial_z K = 0$, we see that $E^T J(\partial_z E)$ is skew symmetric: hence, when the medium is perfectly elastic,

$$\partial_{\sigma}(w^{T}Kw) + \partial_{\sigma}(w^{T}K\Lambda w) = 0, \tag{15}$$

which corresponds to the invariance of vertical power flux.

When M is discontinuous at $z^{(l)}$ the continuity of v implies that

$$E(z^{(l)}+0)w(z^{(l)}+0)-E(z^{(l)}-0)w(z^{(l)}-0)=0.$$
 (16)

By separating the outgoing modes from the incoming modes at $z^{(l)}$, we may rewrite Eq. (16) in terms of a scattering matrix $S^{(l)}$:

$$w_j(z^{(l)} + s_j 0) = \sum_k S_{jk}^{(l)} w_k(z^{(l)} - s_j 0).$$
 (17)

It follows from the conservation of energy flux at $z^{(l)}$ that $S^{(l)}$ is orthogonal.

II. THE INTEGRODIFFERENTIAL EQUATION

In this section we shall derive an integrodifferential equation governing the evolution of the pulse carried by the mode of interest, which we shall assume to be the fastest, for instance, the up- or downgoing P wave in isotropic elasticity.

A. Scaling

In order to estimate systematically the order of magnitude of various terms occurring in the analysis we introduce a small parameter ϵ , $0 < \epsilon < 1$. We shall assume that inhomogeneities in the mechanical parameters are $O(\epsilon)$ while imperfections of elasticity are $O(\epsilon^2)$, but we shall consider wave propagation over large distances $O(\epsilon^{-2})$, so that the effects of these perturbations become appreciable. Let

$$E^{T}(z)J(\partial_{z}E)(z) = \epsilon A(z), \qquad (18a)$$

$$E^{T}(z)J(\partial_{\sigma}M_{1})(z,\sigma)E(z) = \epsilon^{2}B(z,\sigma), \tag{18b}$$

$$S^{(l)} = I - \epsilon \mathcal{A}^{(l)} - \epsilon^2 \mathcal{B}^{(l)}. \tag{18c}$$

It follows from the normalization [Eq. (12)] that the matrix KA is skew, whereas, by Eq. (4), KB is symmetric. The orthogonality of $S^{(l)}$ implies that the O(1) term of $S^{(l)}$ is I, that $\mathcal{A}^{(l)}$ is skew, and that

$$\mathscr{B}_{nn}^{(l)} = \frac{1}{2} \sum_{k=1}^{n-1} \mathscr{A}_{kn}^{(l)^2} = -\frac{1}{2} \sum_{k=1}^{n-1} \mathscr{A}_{kn}^{(l)} \mathscr{A}_{nk}^{(l)}. \tag{19}$$

It is convenient to define $\tau_k(z,z')$ here as the travel time in mode k between z' and z. Thus,

$$\tau_k(z,z') = \int_{z'}^{z} \gamma_k(\zeta) d\zeta. \tag{20}$$

Let (z,θ) be new coordinates related to (z,σ) by

$$\theta(z,\sigma) = \sigma - \tau_n(z,0). \tag{21}$$

In this way we emphasize the *n*th mode as the mode of interest, which, as stated above, we shall take to be the fastest. In these coordinates the diagonal differential operator of Eq. (14) is transformed:

$$K(\partial_z + \Lambda \partial_\alpha) \rightarrow \text{diag}[L_1, ..., L_{n-1}, s_n \partial_z],$$
 (22)

where

$$L_k = s_k (\partial_z + \hat{\gamma}_k \, \partial_\theta), \tag{23}$$

and

$$\hat{\gamma}_k = \gamma_k - \gamma_n. \tag{24}$$

For later use we define

$$\hat{\tau}_{k}(z,z') = \int_{z'}^{z} \hat{\gamma}_{k}(\zeta) d\zeta = \tau_{k}(z,z') - \tau_{n}(z,z').$$
 (25)

Let

$$W(z,\theta) = w_n(z,\sigma) \tag{26}$$

be the amplitude of the mode of interest while we retain $w_k(z,\theta) = w_k(z,\sigma)$ for $1 \le k \le n-1$. Then Eq. (14) may be written

$$s_n \partial_z W + \epsilon \sum_{j=1}^{n-1} A_{nj} w_j + \epsilon^2 B_{nn} * W + \epsilon^2 \sum_{j=1}^{n-1} B_{nj} * w_j = 0,$$
 (27)

for the mode of interest and

 $w_i(z^{(l)}+s_i0,\cdot)-w_i(z^{(l)}-s_i0,\cdot)$

$$(s_{j} \partial_{z} + |\hat{\gamma}_{j}| \partial_{\theta}) w_{j} + \epsilon \sum_{k=1}^{n-1} A_{jk} w_{k} + \epsilon^{2} \sum_{k=1}^{n-1} B_{jk} * w_{k}$$

$$= -\epsilon A_{in} W - \epsilon^{2} B_{in} * W, \qquad (28)$$

with $1 \le j \le n-1$ for the other modes. At interface $z^{(l)}$, we write Eq. (17) as

$$W(z^{(l)} + s_n 0, \cdot) - W(z^{(l)} - s_n 0, \cdot)$$

$$+ \epsilon \sum_{k \neq n} \mathcal{A}_{nk}^{(l)} w_k(z^{(l)} - s_k 0, \cdot) + \epsilon^2 \mathcal{B}_{nn}^{(l)} W(z^{(l)} - s_n 0, \cdot)$$

$$+\epsilon^2 \sum_{k \to n} \mathcal{B}_{nk}^{(l)} w_k(z^{(l)} - s_k 0, \cdot) = O(\epsilon^3), \tag{29}$$

and

$$+\epsilon \mathscr{A}_{jn}^{(l)} W(z^{(l)} - s_n 0, \cdot) + \epsilon \sum_{k \neq n} \mathscr{A}_{jk}^{(l)} w_k(z^{(l)} - s_k 0, \cdot)$$

$$+\epsilon^2 \mathscr{B}_{jn}^{(l)} W(z^{(l)} - s_n 0, \cdot) + \epsilon^2 \sum_{k \neq n} \mathscr{B}_{jk}^{(l)} w_k(z^{(l)} - s_k 0, \cdot)$$

$$= O(\epsilon^3). \tag{30}$$

Equations (27) and (28) are supplemented with initial conditions

$$W(z,\theta) = w_i(z,\theta) = 0, \text{ for } \theta < 0.$$
 (31)

This is possible by consideration of dependence domains, since mode n is the fastest.

B. Perturbation analysis for small ϵ

Let us solve this system by a perturbation method for small ϵ as far as $O(\epsilon^2)$.

Suppose that in a region in z,θ of diameter O(1) containing the point $(z_1,0)$ we may expand W and w_i as

$$W = W^{(0)} + \epsilon W^{(1)} + \epsilon^2 W^{(2)} + O(\epsilon^3), \tag{32}$$

$$w_i = w_i^{(0)} + \epsilon w_i^{(1)} + \epsilon^2 w_i^{(2)} + O(\epsilon^3), \tag{33}$$

with

$$W^{(1)}(z_1,\theta) = W^{(2)}(z_1,\theta) = 0. \tag{34}$$

Then, setting $\epsilon = 0$ in Eqs. (27) and (29), we get

$$\partial_z W^{(0)} = 0$$
 between interfaces, (35)

$$W^{(0)}(z^{(l)}+s.0.\cdot)=W^{(0)}(z^{(l)}-s.0.\cdot)$$

Thus, from Eqs. (35) and (36),

$$W^{(0)}(z,\theta) = W^{(0)}(z^{(l)},\theta) = W(z_1,\theta). \tag{37}$$

Setting $\epsilon = 0$ in Eqs. (28) and (31), we get

$$(s_j \partial_z + |\hat{\gamma}_j| \partial_\theta) w_j^{(0)} = 0$$
 between interfaces, (38)

and

$$w_j^{(0)}(z^{(l)}+s_j0,\theta)-w_j^{(0)}(z^{(l)}-s_j0,\theta)=0$$

at interfaces. (39)

Integrating Eq. (38) along a characteristic of the family

$$d\theta = \hat{\gamma}_i \, dz \tag{40}$$

and making use of Eqs. (39) and (31), we find that

$$w_i^{(0)} = 0. (41)$$

Next we differentiate Eqs. (27) and (29) with respect to ϵ and set ϵ =0:

$$\partial_z W^{(1)} = 0,$$

$$W^{(1)}(z^{(l)} + s_n 0, \cdot) - W^{(1)}(z^{(l)} - s_n 0, \cdot) = 0,$$
(42)

where we have made use of Eq. (41). Integrating Eq. (42) and using Eq. (34) show that

$$W^{(1)} = 0. (43)$$

On differentiating Eqs. (28) and (30) and setting ϵ =0, we find that

$$(s_i \partial_z + |\hat{\gamma}_i| \partial_\theta) w_i^{(1)} = -A_{in} W^{(0)},$$
 (44)

$$w_j^{(1)}(z^{(l)}\!+\!s_j0,\,\,\cdot\,\,)\!-\!w_j^{(1)}(z^{(l)}\!-\!s_j0,\,\,\cdot\,\,)$$

$$= -\mathscr{A}_{in}^{(l)} W^{(0)}(z^{(l)} - s_n 0, \cdot). \tag{45}$$

Then, integrating Eq. (44), adding the contributions from Eq. (45), and taking into account the zero initial conditions [Eq. (31)], we find that

$$w_{j}^{(1)}(z_{1},\theta) = -\int_{\bar{z}_{j}}^{z_{1}} A_{jn}(z') W(z_{1},\theta - \hat{\tau}_{j}(z_{1},z')) dz'$$
$$-\sum_{l}' \mathscr{A}_{jn}^{(l)} W(z_{1},\theta - \hat{\tau}_{j}(z_{1},z^{(l)})), \qquad (46)$$

where we have also used Eq. (37). The lower limit of integration \bar{z}_i is such that

$$\hat{\tau}_i(z_1,\bar{z}_i) = \theta, \tag{47}$$

 $(\bar{z}_j, -0)$ and (z_1, θ) lie on the same j characteristic, and in the summation over l only those terms are included for which $\hat{\tau}_j(z_1, z^{(l)}) < \theta$ (i.e., excluding the end point if that happens to be a point of discontinuity). We may write Eq. (46) in the form

$$w_{j}^{(1)}(z_{1},\theta) = -\int_{\bar{z}_{j}}^{z_{1}} \left(A_{jn}(z') + \sum_{l}' \mathscr{A}_{jn}^{(l)} \delta(z' - z^{(l)}) \right) \times W(z_{1},\theta - \hat{\tau}_{j}(z_{1},z')) dz'. \tag{48}$$

Now we differentiate Eqs. (27) and (29) twice with respect to ϵ , set $\epsilon = 0$, and divide by 2:

$$s_n \, \partial_z W^{(2)}(z_1, \theta) + \sum_{j=1}^{n-1} A_{nj} w^{(1)}(z_1, \theta) + B_{nn} * W(z_1, \theta) = 0,$$
(49)

$$W^{(2)}(z^{(l)}+s_n0,\theta)-W^{(2)}(z^{(l)}-s_n0,\theta)$$

$$+ \sum_{j \neq n} \mathscr{A}_{nj}^{(l)} w_j^{(1)} (z^{(l)} - s_j 0, \theta) + \mathscr{B}_{nn}^{(l)} W(z_1, \theta) = 0.$$
(50)

Notice that on substituting $w^{(1)}$ from Eq. (48) into Eq. (50) the term j=n does not arise in the sum over j. Equations (49) and (50) may be written as the following single equation:

$$s_{n} \partial_{z} W^{(2)}(z_{1}, \theta) + \sum_{j=1}^{n-1} \left(A_{nj}(z_{1}) - \sum_{l}' \mathscr{A}_{nj}^{(l)} \delta(z_{1} - z^{(l)}) \right)$$

$$\times w_{j}^{(1)}(z_{1}, \theta) + B_{nn} * W(z_{1}, \theta) + \sum_{l}' \mathscr{B}_{nn}^{(l)} \delta(z - z^{(l)})$$

$$\times W(z_{1}, \theta) = 0,$$
(51)

provided that we interpret ∂_z in the sense of distributions. We have set $z=z_1$ in Eq. (51), but we shall later drop the subscript 1 on z_1 . On setting $z=z_1$ in Eq. (48) and then substituting in Eq. (51), we obtain $\partial_z W^{(2)}(z_1,\theta)$ in terms of $W(z_1,\theta)$. Equations (32), (35), and (43) yield

$$\partial_z W(z_1, \theta) = \epsilon^2 \, \partial_z W^{(2)}(z_1, \theta). \tag{52}$$

So, setting $z=z_1$, substituting $w_j^{(1)}$ from Eq. (48) into Eq. (51), and then using Eq. (52), we get

$$s_{n} \partial_{z}W(z,\theta) = \epsilon^{2} \left(\sum_{j=1}^{n-1} \bar{A}_{nj}(z) \int_{\bar{z}_{j}}^{z} \bar{A}_{jn}(z') W(z,\theta) - \hat{\tau}_{j}(z,z') dz' - B_{nn} * W(z,\theta) - \sum_{l}' \mathcal{B}_{nn}^{(l)} \delta(z-z^{(l)}) W(z,\theta) \right) + O(\epsilon^{3}),$$

$$(53)$$

where

$$\bar{A}_{jk}(z) = A_{jk}(z) + \sum_{l}' \mathscr{A}_{jk}^{(l)} \delta(z - z^{(l)}).$$
 (54)

There is a slight complication in Eq. (53) when $z=z^{(l)}$, for some l. Then $W(z+s_n0,\theta)-W(z-s_n0,\theta)\neq 0$ and the right side is not well defined. However, this difference is $O(\epsilon^2)$; thus, we may replace $W(z,\theta)$ on the right of Eq. (53) by $W(z+s_n0,\theta)$, $W(z-s_n0,\theta)$, or any value between these, and the equation will remain true to the same order in ϵ . Also, in the product $\bar{A}(z)\bar{A}(z')$, there are terms of the form $\mathcal{A}_{nj}^{(l)}\mathcal{A}_{jn}^{(m)}\delta(z-z^{(l)})\delta(z-z^{(m)})$. But the diagonal terms with m=l do not arise. They appear with a coefficient $\frac{1}{2}$ when Eq. (19) is used in $\mathcal{B}_{nn}^{(l)}\delta(z-z^{(l)})$.

The integrodifferential equation (53) is the main result of this section. We proceed now to write its solution in a convenient form.

C. The solution of the integrodifferential equation

We may rewrite Eq. (53) in the form

$$s_{\cdot \cdot} \partial_z W(z, \cdot) = \epsilon^2 P(z, \cdot) * W(z, \cdot), \tag{55}$$

where

$$P(z,\theta) = \sum_{j=1}^{n-1} \bar{A}_{nj}(z) \int_{\bar{z}_j}^z dz' \, \bar{A}_{jn}(z') \delta(\theta - \hat{\tau}_j(z,z'))$$
$$-B_{nn}(z,\theta) - \sum_{j}' \mathcal{B}_{nn}^{(l)} \delta(z - z^{(l)}) \delta(\theta). \quad (56)$$

The convolution and delay operators appearing in Eq. (56) are mutually commuting (and may be diagonalized by a Fourier or Laplace transform). Let us assume that $s_n=1$; then the solution of Eq. (55) may be expressed as

$$W(z,\cdot) = \exp\left(\epsilon^2 \int_0^z P(z'',\cdot) dz'' *\right) W(0,\cdot), \quad (57)$$

and this equation is valid on a scale of ϵ^{-2} in z with an $O(\epsilon)$ error. [If $s_n = -1$, Eq. (55) must be integrated in the negative instead of the positive z direction.] The exponential is the operator exponential of its argument regarded as a convolution operator in the second slot rather than as a function. This is indicated by the *. We may write the exponent more explicitly. Thus, with an $O(\epsilon)$ error,

$$W(z, \cdot) = \exp[a(z, \cdot)*+b(z, \cdot)*]W(0, \cdot),$$
 (58)

where

$$a(z,\theta) = \sum_{j=1}^{n-1} \int_{0}^{z} \epsilon \overline{A}_{nj}(z'') \int_{\overline{z}_{j}}^{z''} \epsilon \overline{A}_{jn}(z') \delta(\theta)$$
$$-\hat{\tau}_{j}(z'',z') dz' dz''$$
$$-\sum_{\{l|0,c\}^{(l)} \leq z\}} \epsilon^{2} \mathcal{B}_{nn}^{(l)} \delta(\theta), \tag{59}$$

and

$$b(z,\theta) = -\int_0^z \epsilon^2 B_{nn}(z'',\theta) dz''. \tag{60}$$

The convolutions in θ implied by Eq. (58) may be treated conveniently by means of Laplace or Fourier transforms, but when this is done we should be aware of important time-domain considerations relating to causality, which are difficult to treat adequately in the frequency domain.

In the next section we shall show how a and b may be discretized so that Eq. (58) can be treated numerically. We note that the ϵ^2 factors appearing in a and b imply that the approximations are valid on a z scale of ϵ^{-2} .

D. The reflected waves

In practice we need the particle velocities, which are observable quantities. They are components of v, which is related to W and w_i by Eq. (6), and so

$$v = \sum_{i=1}^{n-1} w_i e_j + W e_n. \tag{61}$$

Thus, before calculating v we need to obtain not only W but also the w_j , $1 \le j \le n-1$. But, to leading order in ϵ , w_j is given by Eq. (48) as

$$w_{j}(z,\theta) = -\int_{\bar{z}_{j}}^{z} \epsilon \bar{A}_{jn}(z') W(z,\theta - \hat{\tau}_{j}(z,z')) dz', \qquad (62)$$

where \bar{A}_{jn} is given in Eq. (54). So, finally, using Eq. (62) in Eq. (61), we have

$$v(z,\theta) = -\sum_{j=1}^{n-1} \int_{\bar{z}_j}^{z} \epsilon \bar{A}_{jn}(z') W(z,\theta - \hat{\tau}_j(z,z')) dz' e_j$$

$$+ W(z,\theta) e_n.$$
(63)

Thus, we see that all components of $v(z,\theta)$ are obtained from $W(z,\theta)$ by convolutions in time.

III. THE TRAVEL-TIME CORRECTION AND THE EFFECTIVE MEDIUM

The effect of the heterogeneity of the medium as represented by $a(z, \cdot)$ in (58) is twofold: a delay in the pulse, and an evolution of the pulse shape, usually a broadening. It turns out that the delay is $O(\epsilon^2)$ and to this order is the same as the delay calculated by means of an effective medium theory. The delay and the effective medium will be made precise in the course of the discussion.

The delay $\Delta t(z)$ of the pulse after the leading characteristic may be defined as the centroid in θ of the pulse $W(z,\theta)$. It is given by the equation

$$\int_0^\infty \theta W(z,\theta) d\theta = \Delta t(z) \int_0^\infty W(z,\theta) d\theta. \tag{64}$$

Let $\hat{f}(z,s)$ be the Laplace transform in θ of $f(z,\theta)$:

$$\hat{f}(x,s) = \int_0^\infty e^{-s\theta} f(z,\theta) d\theta. \tag{65}$$

Then

$$\int_0^\infty f(z,\theta)d\theta = \hat{f}(z,0),$$

$$\int_0^\infty \theta f(z,\theta)d\theta = -\hat{f}_s(z,0).$$
(66)

Laplace-transforming (58), and assuming for the present purpose that $b(z,\theta) = 0$, we have

$$\hat{W}(z,s) = \exp[\hat{a}(z,s)] \hat{W}(0,s),$$
 (67)

and so, on differentiating and using the fact that $\hat{a}(z,0) = 0$,

$$\hat{W}_{s}(z,0) = \hat{a}_{s}(z,0)\,\hat{W}(z,0). \tag{68}$$

Thus, using (64) and (66) in (68), we get

$$\Delta t(z) = -\hat{a}_{s}(z,0)$$

$$=\int_0^\infty \theta a(z,\theta)d\theta$$

$$=\epsilon^2\sum_{j=1}^{n-1}\int_0^z \bar{A}_{nj}(z'')\int_{\bar{z}_j}^{z''} \bar{A}_{jn}(z')\tau(z'',z')dz'dz'',$$

(69)

by (59).

On the other hand, an effective medium over the interval $(0,z_0)$ may be defined by replacing M $(=M_0)$ in (1) by

$$\langle M_0 \rangle_{z_0} = \frac{1}{z_0} \int_0^{z_0} M_0(z) dz.$$
 (70)

It will not be demonstated here, but may be shown by direct calculation, that the characteristic travel time from 0 to z_0 in this effective medium is larger than the characteristic travel time $\tau(0,z_0)$ by $\Delta t(z_0)$, correct to $O(\epsilon^2)$, which is the result stated at the beginning of this section.

IV. SIMULATIONS

A. Discretization

In general, when both jumps and continuous variation of the medium occur, it is convenient to discretize $\bar{A}_{jn}^{(l)}$ on a uniform grid in z with step d, say. Then, in the integrals, $\bar{A}_{jn}^{(l)}$ dz becomes

$$\alpha_{jn,m} = A_{jn}(z_m)d + \sum_{l} \mathscr{A}_{jn}^{(l)}, \qquad (71)$$

where the second term arises only if $z_m - \frac{1}{2}d \leqslant z^{(l)} < z_m + \frac{1}{2}d$. Then, to discretize $a(z,\theta)$ of (59) we discretize θ with step size h and sample intervals $[(q-\frac{1}{2})h,(q+\frac{1}{2})h)$. Set $a_q=0$. Fix z. Then, for each admissible pair m, m', find q' such that

$$(q' - \frac{1}{2})h \leqslant \hat{\tau}_j(z_m, z_{m'}) < (q' + \frac{1}{2})h. \tag{72}$$

We accumulate $a_{\alpha'}$ by adding a term as follows:

$$a_{o'} \leftarrow a_{o'} + \epsilon^2 \alpha_{ni,m} \alpha_{in,m'} h. \tag{73}$$

In addition, for q'=0, we add the contribution from $\mathcal{B}_{nn}^{(l)}$ of (59):

$$a_0 \leftarrow a_0 - \sum_{\{l \mid 0 < z^{(l)} < z\}} \epsilon^2 \mathcal{B}_{nn}^{(l)}.$$
 (74)

The quantity $b(z,\theta)$ may be discretized in θ for fixed z by any numerical quadrature formula (in z) and at the same discretization points $\theta = qh$ as for a_q . Thus in the crudest approximation,

$$b_q = -\int_0^z \epsilon^2 B_{nn}(z'',hq)dz''. \tag{75}$$

We can form the sum

$$c_a = a_a + b_a \tag{76}$$

and its generating function

$$C(\xi) = \sum_{q=0}^{\infty} c_q \xi^q.$$
 (77)

It is now possible to compute the convolutional exponential $\{u_a\}$ of $\{c_a\}$ as follows:

$$U(\xi) = \sum_{q=0}^{\infty} u_q \xi^q = \exp[C(\xi)]. \tag{78}$$

Differentiate with respect to ξ to get

$$U'(\xi) = U(\xi)C'(\xi),\tag{79}$$

that is.

$$\sum_{m=1}^{\infty} m u_m \xi^{m-1} = \sum_{m=1}^{\infty} \sum_{q=1}^{m} q u_{m-q} c_q \xi^{m-1}.$$
 (80)

Thus u_m may be computed recursively by means of

$$u_{m} = \frac{1}{m} \sum_{q=1}^{m} q c_{q} u_{m-q}. \tag{81}$$

The recursion needs to be started at m=0 by

$$u_0 = e^{-a_0}. (82)$$

The sequence $\{u_m\}$ may also be computed by means of the Fourier transform. This is more efficient provided wraparound errors are avoided. For Goupillaud media and normal incidence the Fourier transform of the autocorrelation function of reflection coefficients is easily and rapidly computed from the reflection coefficient sequence and leads to a very fast algorithm, which is 30–30 000 times faster than competing methods, depending on the number of receivers, the number of layers the waves must traverse, the lengths of the time series to be computed, and the frequency content of the incident wave.

B. Results

Synthetic media were constructed consisting of a stack of a large number of homogeneous layers. The statistics

were governed by fractional Brownian motion with Hurst exponent H. The relationship of H to the fractional Brownian motion will be specified later in (86); H can be expressed in terms of the fractal (box) dimension D by means of

$$H=2-D. (83)$$

There is evidence⁸⁻¹⁰ that actual media show power spectral densities arising from this class of stochastic fractal. Here, we summarize some of the basic relations among the fractal, its power spectral density, its autocorrelation function, the realization it generates, and the resulting reflectivity sequence.

We shall be concerned with normally incident plane waves. Let $\xi^{(v)}(z)$ be the stochastic process for the acoustic impedance v. For the time being we will consider ensemble averages (\mathscr{E}), but later on we will focus on a particular realization. The variogram \mathcal{V}_{ν} , of $\xi^{(\nu)}$ is given by

$$\mathscr{V}_{\nu}(\zeta) = \mathscr{E}\{|\xi^{(\nu)}(\cdot + \zeta) - \xi^{(\nu)}(\cdot)|^2\}. \tag{84}$$

It is related to the power spectral density \mathcal{P}_{vv} , by

$$\mathscr{V}_{\nu}(\zeta) = \int_{0}^{\infty} \left[1 - \cos(k\zeta) \right] \mathscr{P}_{\nu\nu}(k) dk, \tag{85}$$

through the spatial Fourier transformation \mathcal{F} . Here k is the wave number conjugate to z. For fractional Brownian motion the power spectral density is related to the Hurst exponent by the simple power law

$$\mathcal{P}_{\mathcal{W}}(k) = C_H / k^{2H+1}, \tag{86}$$

where C_H is a coefficient, depending upon H and the length of the process, which normalizes the variance to 1. Then the variogram is stationary. If the Fourier inverse exists, and $\xi^{(\nu)}$ is stationary, we have

$$(\mathcal{F}^{-1}\mathcal{P}_{\nu\nu})(\zeta) = \mathcal{E}\{\xi^{(\nu)}(\cdot)\xi^{(\nu)}(\cdot+\zeta)\} = c_{\nu\nu}(\zeta),$$
(87)

where c_{yy} denotes the autocorrelation function. Then the correlation function of the derived process $\xi^{(v)}$, (associated with the reflectivity function) is

$$\mathscr{E}\{\xi^{(\nu)}, (\cdot)\xi^{(\nu)}, (\cdot+\zeta)\} = -c_{\nu\nu}''(\zeta). \tag{88}$$

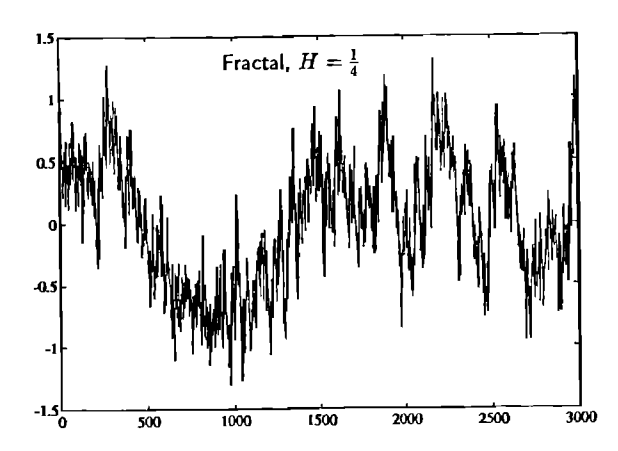


FIG. 1. A fractional Brownian motion fractal with Hurst exponent $H=\frac{1}{4}$ used to generate the reflection coefficient sequences shown in Figs. 2 and 7 through formula (92).

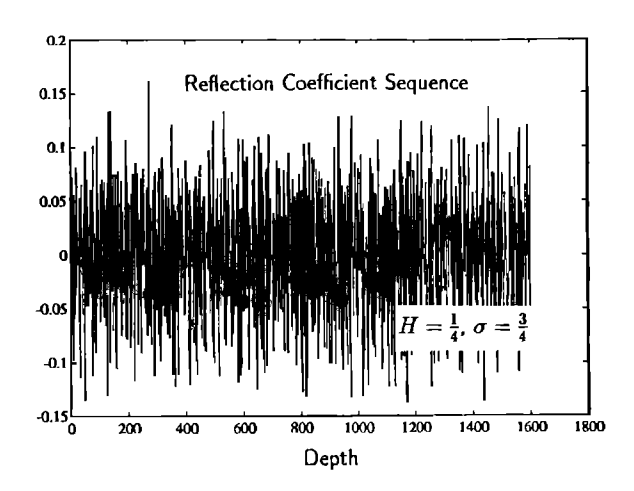


FIG. 2. The reflection sequence generated from the fractal shown in Fig. 1 using formula (29) with $\sigma_v = \frac{3}{4}$.

For $0 < H < \frac{1}{2}$, the left member of (88) exists even though c_{yy} does not. We then regard (88) as defining c''_{yy} , which will need to be interpreted as a distribution. At zero lag we

$$\mathscr{E}\{\xi^{(\nu)}(\,\cdot\,)\xi^{(\nu)}(\,\cdot\,)\} = \int_{-\infty}^{\infty} \mathscr{P}_{\nu\nu}(k)dk. \tag{89}$$

This implies, through the Wiener-Khinchine theorem, that

$$\mathscr{P}_{\nu\nu}(k) = \mathscr{E}\{(\mathscr{F}\xi^{(\nu)})(\mathscr{F}\xi^{(\nu)})^*\}(k). \tag{90}$$

The latter relation, without the averaging, was used to construct a fractional Brownian motion from a random process by enforcing the desired power spectral density (86).

For the more general case of oblique incidence, several parameters need to be generated. Then (85)-(90) may be simply extended to cover covariances and the generation of

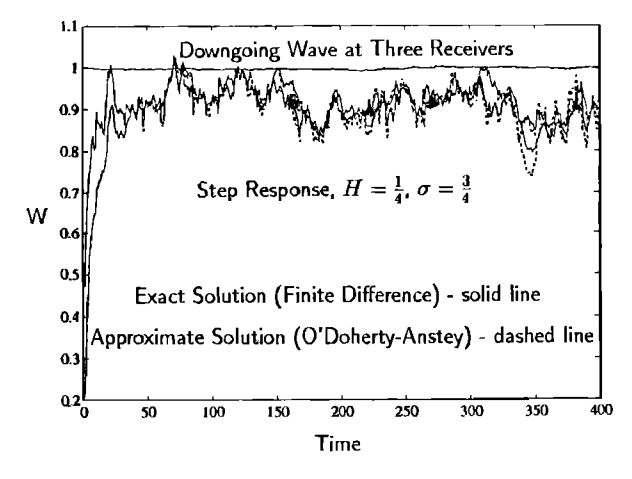


FIG. 3. The downgoing wave response to a unit step function pulse incident from above on a stack of layers with reflection coefficient sequence shown in Fig. 2. There are three pairs of curves showing the pulse at three receiver locations: in the 1st layer (just below the top interface), in the 601st layer, and in the 1201st layer. For each receiver, the solid line depicts the exact solution as calculated by means of a discrete solver for a Goupillaud medium, and the dashed line the approximation computed according to (58). Toward the left of the figure the curves corresponding to the three receivers are lower the deeper the receiver. The curves for the first receiver both almost coincide with the line W=1. $H=\frac{1}{4}$ and $\sigma_v=\frac{3}{4}$.

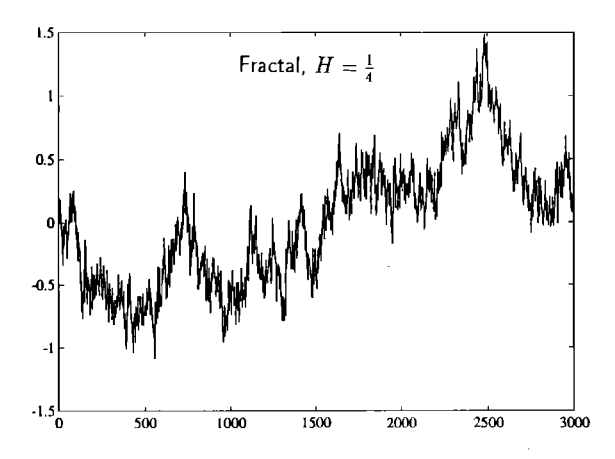


FIG. 4. A fractional Brownian motion fractal with Hurst exponent $H=\frac{1}{4}$ used to generate the reflection coefficient sequences shown in Fig. 5 through formula (92).

the $c_{\mu\nu}^{\prime\prime}$, provided that the fractal dimension is the same for all parameters. For practical purposes the discretization $\xi_k^{(\nu)}$ of the process $\xi^{(\nu)}$ implies a natural high wave-number band limitation of the power spectral density since the sampling rate is to be regarded as the Nyquist wave number. The finite support of the process implies a band limitation with respect to the low wave numbers.

Once $\xi_k^{(v)}$ is generated, the sequence of characteristic impedances $\{v_k\}$ may be generated by means of

$$v_k = \exp(\sigma_k \xi_k^{(v)}), \tag{91}$$

where σ_{ν} governs the magnitude of the reflection coefficients $\{r_k\}$, which are given by

$$r_k = \tanh\left[\frac{1}{2}\sigma_v(\xi_{k+1}^{(v)} - \xi_k^{(v)})\right].$$
 (92)

We consider two classes of models: in one class, $H=\frac{1}{4}$, and, in the other, $H=\frac{3}{4}$. The first synthetic structure consists of a stack of 1600 layers with $H=\frac{1}{4}$ and $\sigma_v=\frac{3}{4}$. Plots of the underlying fractal and the reflection coefficients are shown in Figs. 1 and 2. The impedance is not stationary although the reflection coefficients are.

In the model, receivers were placed at three locations: in the 1st, the 601st, and the 1201st layers. For each re-

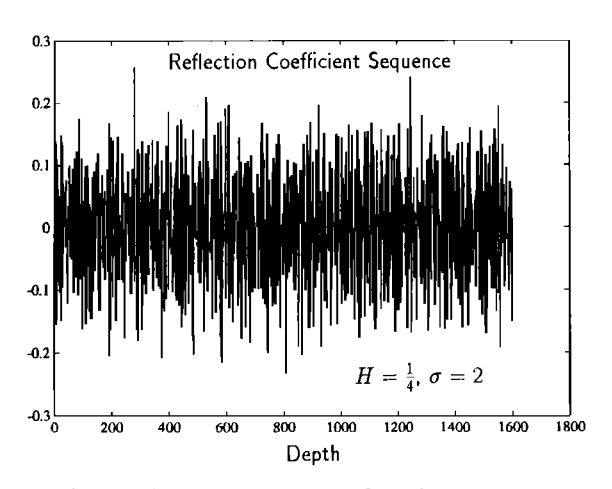


FIG. 5. The reflection sequence generated from the fractal shown in Fig. 4 using formula (92) with $\sigma_v = 2$.

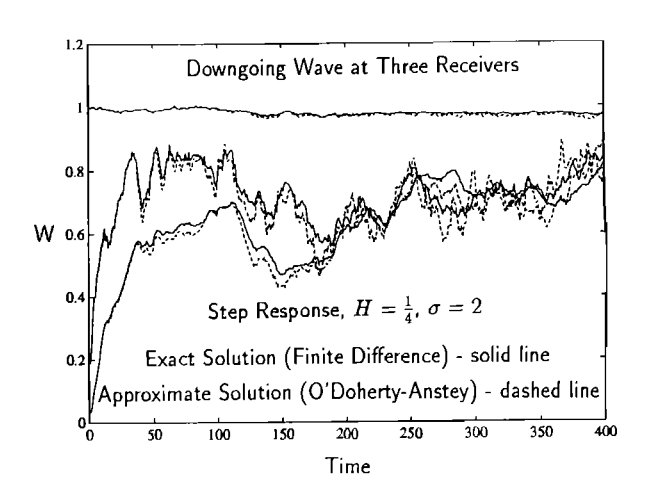


FIG. 6. As in Fig. 3, we show the downgoing wave response to a unit step function pulse incident from above on a stack of layers, but with the reflection coefficient sequence shown in Fig. 5. The results are shown for the same receiver positions as before. Here $H = \frac{1}{4}$ and $\sigma_v = 2$.

ceiver the approximate downgoing wave was computed. The exact downgoing wave was computed with a finite difference code. The results are plotted in Fig. 3. Next we increase σ_v to 2. A different realization was used but with the same value of H. Plots of the fractal and the reflection coefficients are shown in Figs. 4 and 5. Both the exact and the approximate downgoing waves are plotted in Fig. 6. Note that the pulse is broader the larger the value of σ_v and the deeper the point of observation. However, the validity of the approximate method breaks down at earlier times. To illustrate this an extreme case with $\sigma_v=4$ is plotted in Fig. 7 (the fractal realization of Fig. 1 used). The results are plotted in Fig. 8.

A realization of the second class, with $H=\frac{3}{4}$, is shown in Fig. 9; the corresponding reflectivity, with $\sigma_v=15$, is plotted in Fig. 10. Here σ_v was chosen so that a_0 [see (74)] has the same value as for the case $H=\frac{1}{4}$ and $\sigma_v=2$. The strength of the reflection coefficients is comparable with those shown in Fig. 2. Figure 11 shows the exact and the approximate downgoing waves. Notice that there is no broadened pseudoprimary pulse in this case, only the ex-

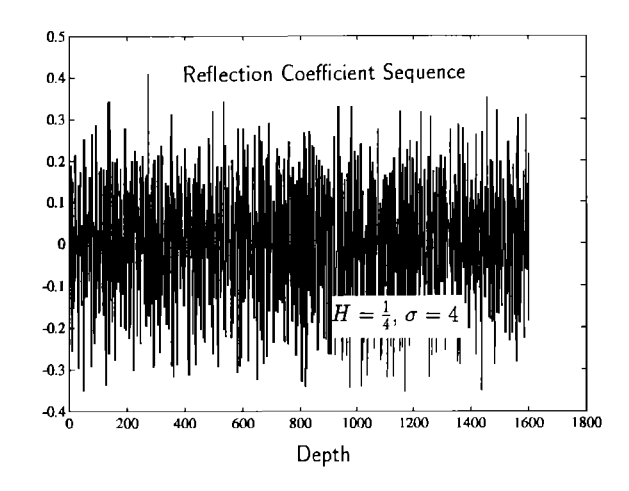


FIG. 7. The reflection sequence generated from the fractal shown in Fig. 1 using formula (92), $\sigma_v = 4$.

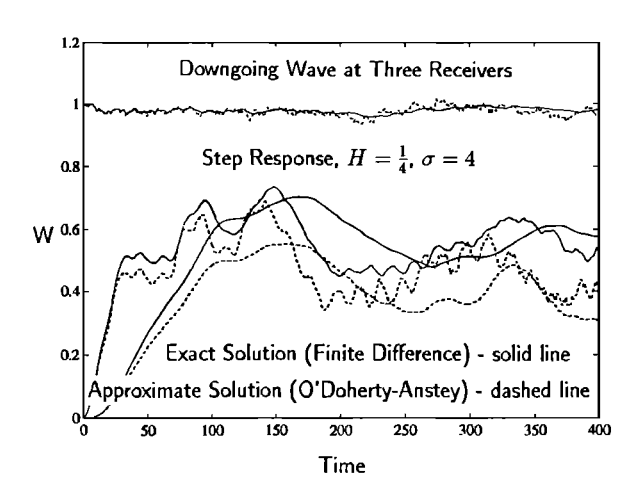


FIG. 8. As in Fig. 3, we show the downgoing wave response to a unit step function pulse incident from above on a stack of layers, but with reflection coefficient sequence shown in Fig. 7. The results are shown for the same receiver positions as before. Here $H = \frac{1}{4}$ and $\sigma_v = 4$.

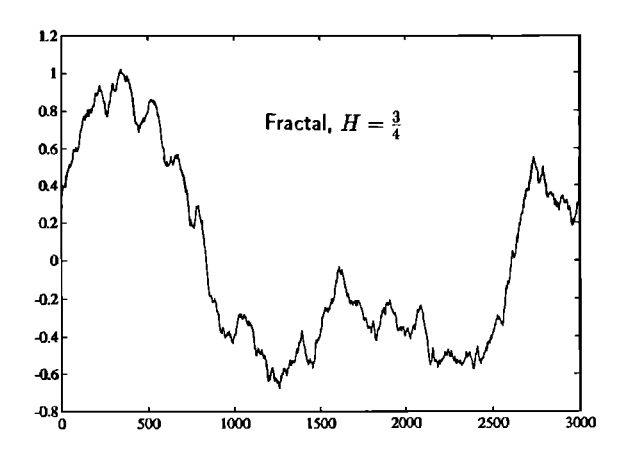


FIG. 9. A fractional Brownian motion fractal with Hurst exponent $H=\frac{3}{4}$ used to generate the reflection coefficient sequences shown in Fig. 10 through formula (92).

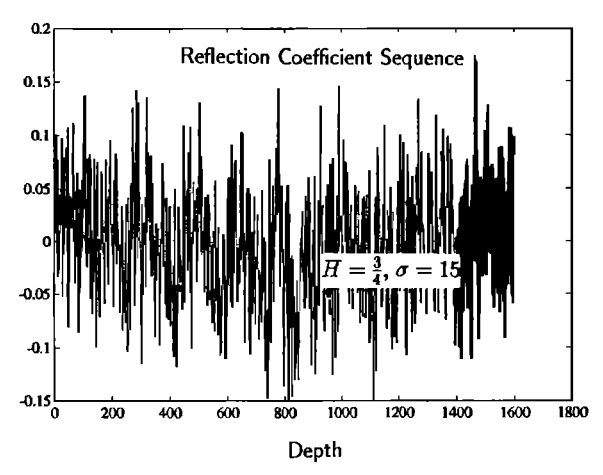


FIG. 10. The reflection sequence generated from the fractal shown in Fig. 9 using formula (92) with $\sigma_v = 15$.

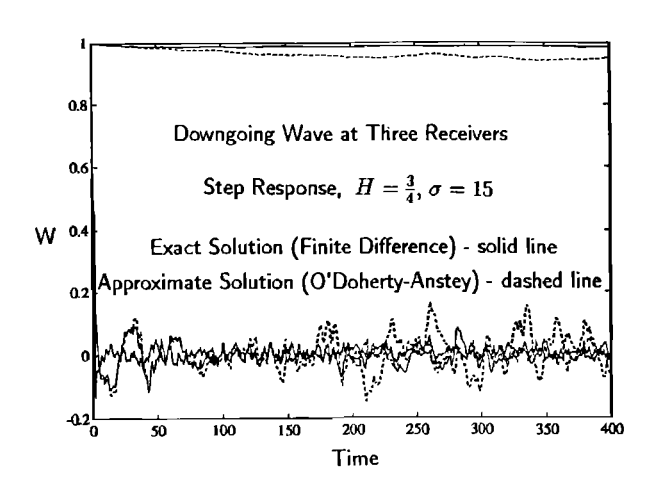


FIG. 11. As in Fig. 3, we show the downgoing wave response to a unit step function pulse incident from above on a stack of layers having the reflection coefficient sequence shown in Fig. 10. The results are shown for the same receiver positions as before, in the 1st, 601st, and 1201st layers. Here $H=\frac{3}{4}$ and $\sigma_v=15$.

ponentially decreasing first arrival, followed by an incoherent coda. This is to be contrasted with the pulses shown in Figs. 3 and 6.

For $0 < H < \frac{1}{2}$, neighboring values of the reflectivity are negatively correlated; then a pseudoprimary wave exists (see Figs. 3 and 6). For $\frac{1}{2} < H < 1$ neighboring values of the reflectivity are positively correlated; then the pseudoprimary wave vanishes (see Fig. 11).

Next we consider the backscattered signal. Here we

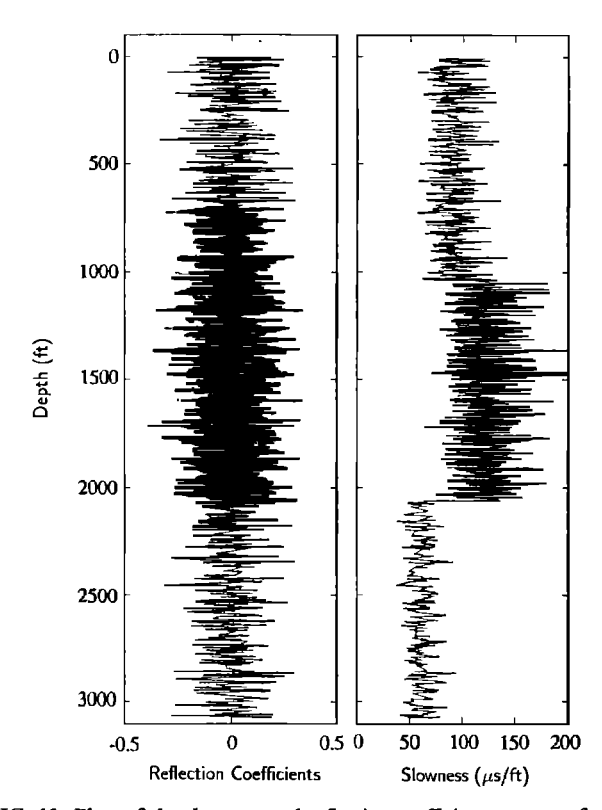


FIG. 12. Plots of the slowness and reflection coefficient sequence for the structure used in the computation of the solutions shown in Figs. 13 and 14. The structure consists of three distinct sections that are statistically stationary. The density was assumed constant.

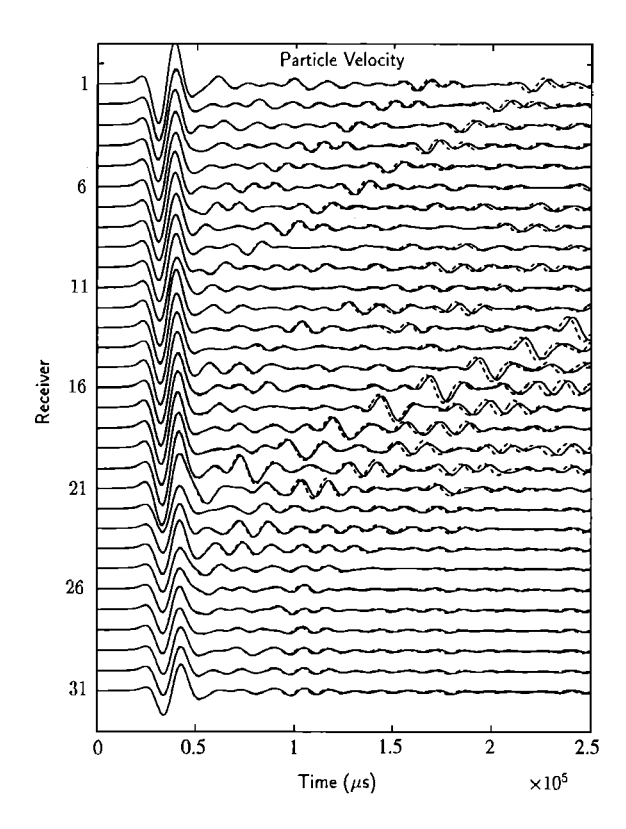


FIG. 13. Particle velocity, which is a linear combination of upgoing and downgoing waves, as a function of time at 31 different receiver positions for the model illustrated in Fig. 12. The incident pulse is broad here (low frequency) and is seen at the beginning of the first trace. This simulation is pushed further into the coda than in the preceding examples. Again solid lines represent the "exact" solution, computed by means of the layer-matrix code OASES, and the dashed lines represent the approximate solution using the method of this paper.

use a smooth source signature rather than a step function in time to investigate the effect for longer wavelengths. The medium, consisting of 3000 layers, is shown in Fig. 12. The upgoing wave was approximated, according to (62), and the particle velocity \bar{v} , say, was computed according to (63). To compare with an exact solution a layer matrix code was run for the same structure and the same incident waveform; the (exact) particle velocities $v(z,\theta)$ were then computed as functions of time at 31 receivers spaced at intervals of 100 layers. Both sets of waveforms $\bar{v}(z,\theta)$ (dashed line) and $v(z,\theta)$ (solid line) are plotted in Fig. 13. Note that the agreement is close but there is a small progressive error in timing as time increases. To improve the approximate results at later times (and hence for the backscattered waves) we introduce in Eqs. (59) and (62) a correction to $\hat{\tau}_j(z',z'')$, the vertical travel time delay for double-scattering between z'' and z', by emphasizing the timing of the centroids of the pulses rather than the characteristic travel time, even for the short propagation paths involved in the double scattering process. Thus, to bring the timing of the centroids into agreement with the longwavelength equivalent medium (as for the primary pulse) we replace the quantities $\hat{\tau}_i(z',z'')$ by

$$\hat{\tau}_{j}(z',z'') \to \langle \tau_{j} \rangle (z',z'') - \langle \tau_{n} \rangle (z',z''), \tag{93}$$

where $\langle \cdot \rangle$ refers to the equivalent medium for the interval

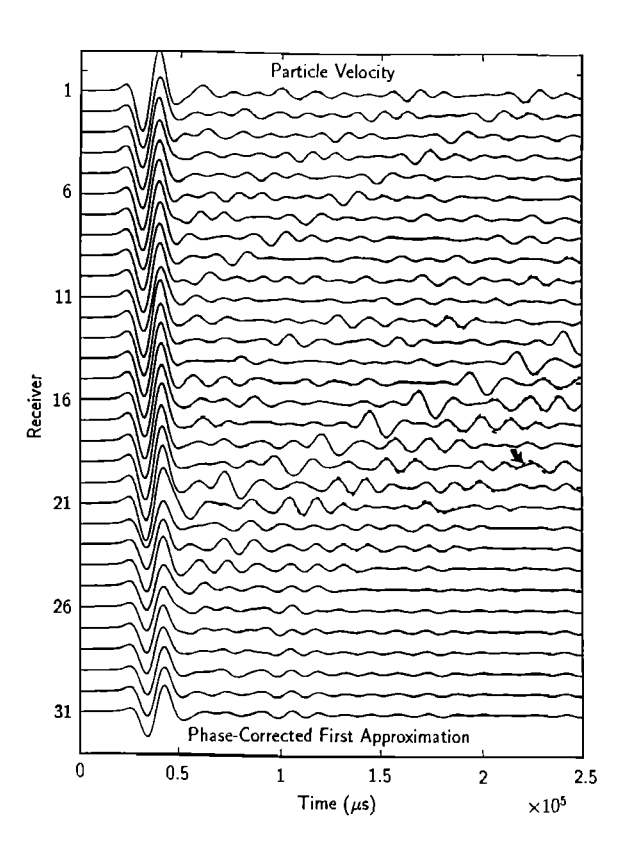


FIG. 14. Same as Fig. 13 except that in the computation of the approximate solution all travel times were calculated relative to the effective medium. Note that errors of timing are now corrected.

[z'',z']. This assumes that the pulse shape of the multiple is similar to that of the primary. Further, the timing of the head of the primary pulse is not affected by the replacement (93) since the correction is $O(\epsilon^2 \theta)$ and only becomes appreciable at later times, $\theta = O(\epsilon^{-2})$. Figure 14 shows the result of using the effective medium timing instead of $\hat{\tau}_i(z'',z')$ throughout in computing $a(z,\theta)$ in Eq. (59). Notice that the agreement between the two solutions is excellent, especially for early times where their graphs are seen to coincide. Some slight difference is found at later times. The computation of the approximate solution \bar{v} was one to three orders of magnitude faster than the layer-matrix computation. We note the coherent up- and downgoing waves (pseudomultiples) that appear to have been reflected from the interior of the stack of layers, presumably where some favorable correlation between the downgoing wave and the structure occurs.

¹R. Burridge and H.-W. Chang, "Multimode one-dimensional wave propagation in a highly discontinuous medium," Wave Motion 11, 231-249 (1989).

²M. V. de Hoop, R. Burridge, and H.-W. Chang, "Wave propagation with tunneling in a highly discontinuous medium," Wave Motion 13. 307-327 (1991).

³R. F. O'Doherty and N. A. Anstey, "Reflections on amplitudes," Geophys. Prosp. 19, 430-458 (1971).

⁴P. G. Richards and W. Menke, "The apparent attenuation of a scattering medium," Bull. Seism. Soc. Am. 73, 1005-1021 (1983).

⁵R. Burridge, B. White, and G. Papanicolaou, "One-dimensional wave propagation in a highly discontinuous medium," Wave Motion 10, 19-44 (1988).

- ⁶R. Burridge, "Waves in finely layered media," in Applied and Industrial Mathematics, edited by R. Spigler (Kluwer Academic, Amsterdam, 1991), pp. 267-279.
- ⁷M. Asch, W. Kohler, G. Papanicolaou, and B. White, "Frequency content of randomly scattered signals," SIAM Rev. 33, 519-625 (1991).
- ⁸A. T. Walden and J. W. J. Hosken, "An investigation of the spectral
- properties of primary reflection coefficients," Geophys. Prosp. 33, 400-435 (1985).
- ⁹J. Feder, *Fractals* (Plenum, New York, 1988).
- ¹⁰F. J. Herrmann and C. P. A. Wapenaar, "Macro description of fine layering: Proposal for an extended macro model," Extended Abstracts, Sixty-Second Annual International Meeting, Society of Exploration Geophysicists, New Orleans, 1992.